ACS OMEGA

Article

Cite This: ACS Omega 2019, 4, 12575−12583

http://pubs.acs.org/journal/acsodf

Red-Emissive Carbon Dots for "Switch-On" Dual Function Sensing Platform Rapid Detection of Ferric Ions and L-Cysteine in Living Cells

Xingxing Yang,[†] Fangchao Cui,[†] Rong Ren,[‡] Jiadi Sun,*[,†] Jian Ji,[†] Fuwei Pi,[†] Yinzhi Zhang,[†] and Xiulan Sun*[,†]

[†]State Key Laboratory of Food Science and Technology, School of Food Science and Technology, National Engineering Research Center for Functional Foods, School of Food Science Synergetic Innovation Center of Food Safety and Nutrition, Jiangnan University, Wuxi, Jiangsu 214122, China

[‡]School of Foreign Studies, Shaanxi University of Technology, Hanzhong, Shaanxi 723000, People's Republic of China

Supporting Information

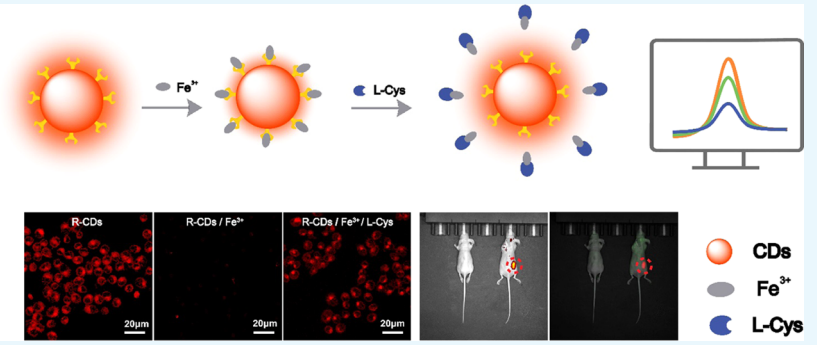

ABSTRACT: Ferric ions (Fe^{3+} ions) and L-cysteine ((L-Cys) in the human body have always played an irreplaceable role in biological processes, and overload or deficiency of Fe^{3+} ions and L-Cys in the biological system leads to various diseases. In this work, N,S-co-doped red-emitting carbon dots (R-CDs) were synthesized by a facile hydrothermal method. Because the doping of N and S gives a unique functional group distribution on the surface of R-CDs, it can be complexed with Fe^{3+} ions to construct an energy transfer quenching system. However, the presence of L-Cys competitively binds to Fe^{3+} ions, thus resulting in the photoluminescence recovery of R-CDs. Therefore, a "switch-on" dual function sensing platform has successfully been developed based on R-CDs for rapid identification and quantification of Fe^{3+} ions and L-Cys. The linear detection range of Fe^{3+} ions is 0−30 μM (limit of detection (LOD): 0.27 μM) and that of L-Cys is 0−24 μM (LOD: 0.14 μM). The sensor platform was used to detect Fe^{3+} ions and L-Cys in human serum samples with satisfactory results. Compared with traditional detection methods, this method is more time-saving and efficient and can be completed in 3 min. It is worth mentioning that the R-CDs not only has high optical stability but also has negligible cytotoxicity and has been successfully applied to in vitro/vivo imaging, indicating that R-CDs have excellent tissue penetration and biomarker potential. More interestingly, the switch-on fluorescence behavior for stepwise detection of Fe^{3+} ions and L-Cys can also be observed in cell imaging, which provides the possibility of visual detection of the probe to be applied in vivo.

1. INTRODUCTION

Trace metals and thiol-containing amino acids in the human body have always played an irreplaceable role in biological processes. Therefore, they have been widely concerned by researchers. In particular, Fe^{3+} ions are essential trace elements in organisms and play a vital role in body metabolism. L-Cys is mainly involved in maintaining the homeostasis of physiological redox in the body, and overload or deficiency of Fe^{3+} ions and L-Cys in the biological system leads to various diseases (cardiovascular disease, anemia, heart failure, diabetes, etc.).[1−4] In addition, the occurrence of cerebrovascular diseases is related to both Fe^{3+} ions and cysteine. In view of the above situation, rapid identification and quantification of them is very necessary.

Currently, there are many methods for quantitatively detecting Fe^{3+} ions and L-Cys. These methods mainly include inductively coupled plasma mass spectrometry (ICP-MS),[5] inductively coupled plasma-atomic emission spectrometry (ICP-AES),[6] atomic absorption spectrometry, membrane separation,[7] chromatographic separation,[8] and capillary electrophoresis.[9] Although these methods are widely used, the disadvantages such as time consuming, cumbersome operation, expensive equipment, poor selectivity, and low detection efficiency are in urgent need of improvement. Therefore, the development of a fast, accurate, environment-friendly, and

Received: April 9, 2019
Accepted: June 24, 2019
Published: July 24, 2019

DOI: 10.1021/acsomega.9b01019
ACS Omega 2019, 4, 12575−12583

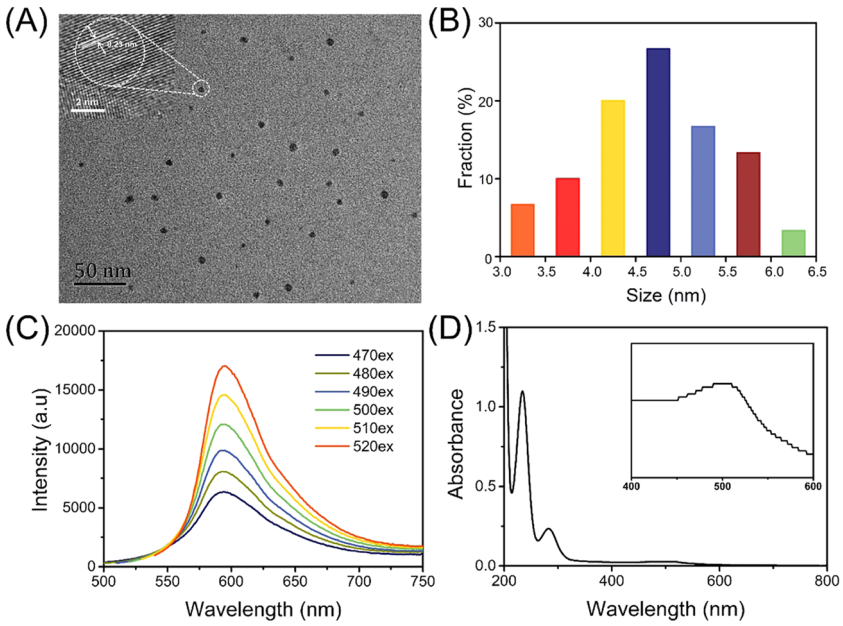

Figure 1. TEM and HRTEM (inset) images of the R-CDs (A). Particle size distributions of the R-CDs (B). FL emission spectra of the R-CDs at different excitation wavelengths (C). UV−vis absorption spectra of the R-CDs dispersed in water (D).

rapid sensing platform for Fe^{3+} ions and L-Cys is of great significance.

Fluorescent probe-based chemical probes have outstanding performance in terms of rapid response, easy operation, and specific recognition. In particular, when carbon dots (CDs) are used as fluorescent probes, they not only have good optical properties but also are environmentally friendly chemical sensing platforms. Compared to fluorescent dyes and semiconductor quantum dots (QDs), CDs have significant advantages in terms of photobleaching resistance, low cost, and biocompatibility. CDs have been widely researched in recent years for potential applications in biosensing, biomedical, catalysis, and optoelectronic devices.[10−15] Many types of heteroatom-doped CDs have been prepared, and they are widely used in sensing. However, most sensing platforms display emission only in short wavelength regions under UV excitation.[16] Therefore, previously reported fluorescent probes based on heteroatom-doped CDs have been difficult to apply to biologically relevant fields. For example, Huang et al. synthesized nitrogen-doped blue CQDs, which could be used as determination elements for the detection of L-Cys.[17] According to Chen et al., blue-emitting tea-CDs obtained by using waste tea extract as a carbon source, as an "on−off−on" fluorescent nanosensor of the tea-CDs, can be used for sensitive detection of CrO_4^{2-}, Fe^{3+}, AA, and L-Cys.[18] Zhang et al. prepared blue-emitting CDs using citric acid as a carbon source and ammonia solution as a nitrogen source, which can be developed into an effective fluorescence sensing platform for detecting L-Cys.[19] First, compared to the reported CDs,[20−23] R-CDs not only have good tissue penetration but also are easier to prepare. Therefore, it is more suitable for detection in vivo. Second, Qu et al. developed a glutathione-based functionalized graphene quantum dot for the identification of Fe^{3+} ions.[24] In contrast, it is simpler than the method of imparting a special surface state of CDs by doping of heteroatoms for identifying Fe^{3+} ions. Third, red-emitting aqueous phase CDs were synthesized by a one-step hydrothermal method, which is safer for detection of Fe^{3+} ions in living cells than red-emitting sulfur, nitrogen codoped carbon dots synthesized with an organic phase.[25] Fourth, Ding et al. synthesized B,N,S-co-doped red-emitting CDs using two raw materials, and used it for detection of Fe^{3+} ions in complex biological fluids and living cells.[26] This work synthesized N,S-co-doped red-emitting CDs using only one raw material. In contrast, the preparation procedure is simpler and cheaper, and the fluorescent probe based on the R-CDs can detect Fe^{3+} ions and can also detect L-Cys in living cells. Finally, it is worth mentioning that this method is more time-saving, more efficient, and can be completed in a few minutes compared to the traditional detection methods.

In this study, red luminescent CDs codoped with sulfur and nitrogen was prepared by a facile hydrothermal method using 2,5-diaminobenzenesulfonic acid as the unique carbon precursor. R-CDs exhibit excellent monodispersity, photobleaching resistance, storage resistance, and biosafety, and more importantly, emit excitation-independent bright red fluorescence for imaging in vivo and in vitro. What is more interesting is that the CDs can be used to construct a dual-functional sensing platform for ultrasensitive real-time detection of Fe^{3+} ions and L-Cys. It is worth mentioning that the "switch-on" fluorescence behavior for cell imaging by reacting with Fe^{3+} ions and L-Cys, respectively, has been investigated. Finally, the sensor platform was used to detect Fe^{3+} ions and L-Cys in human serum samples with satisfactory results.

2. RESULTS AND DISCUSSION

2.1. Characterization and Optical Properties of R-CDs. R-CDs were prepared by a facile hydrothermal method using 2,5-diaminobenzenesulfonic acid as the sole raw material. Characterization of particle size and morphology was determined by transmission electron microscopy (TEM) and high-resolution TEM (HRTEM). As shown in Figure 1A,B, the as-prepared R-CDs are well dispersed spherical particles and the size is uniformly distributed between 3 and 7 nm with an average diameter of about 4.88 ± 0.4 nm. The HRTEM

DOI: 10.1021/acsomega.9b01019
ACS Omega 2019, 4, 12575−12583

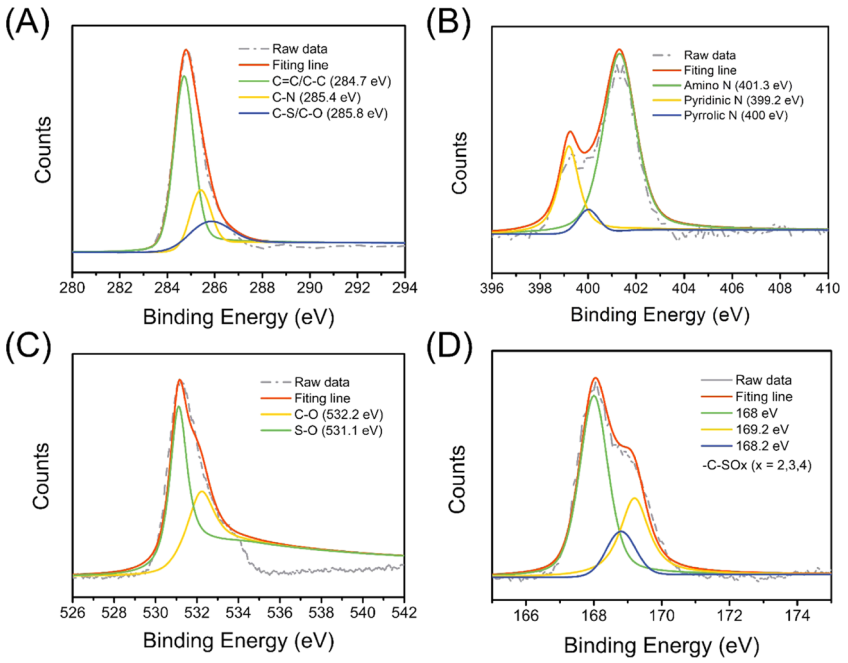

Figure 2. High-resolution C 1s spectra (A), N 1s spectra (B), O 1s spectra (C), and S 2p spectra (D) of the R-CDs.

image shows high crystallinity with a lattice fringe distance of 0.23 nm, corresponding to the (100) lattice plane of graphene. The dry solid R-CD samples were then further characterized using X-ray diffraction (XRD) and Raman spectra. The XRD pattern, as shown in Figure S2A, exhibits a peak at 25.6°, which is the characteristic (002) diffraction peak of graphite. Figure S2B illustrates the Raman spectra of the R-CDs, showing two peaks at 1352 (D band) and 1574 cm^{-1} (G band), and the ratio of I_D/I_G is 1.19. As is known, the ratio of I_D/I_G characterizes the degree of graphitization of the R-CDs. Uniform particle size and good dispersibility indicate that the as-prepared R-CDs exhibit excellent optical properties. As shown in Figure 1C, the R-CDs emitting at around 593 nm showed an excitation-independent feature, underlying the excitation wavelength of 470−520 nm. This is probably due to the fact that in larger CDs, the fluorescence emission is determined by the size of the carbon skeleton, so that the CDs with uniform particle size distribution exhibit excitation-independent fluorescence properties, which is consistent with the research findings of Zhang et al.[27] In Figure 1D, the UV spectrum exhibits two absorption peaks at 283 and 234 nm, which may be attributed to the $\pi-\pi^*$ transition of C═N and C═C bonds. Also, there was a broad absorption band at about 510 nm due to the surface state defects caused by the doping of S and N. The absorption peak at 510 nm is close to the excitation wavelength. Such a unique absorption feature imparts red emission characteristics to the R-CDs.

To further study the fluorescence stability of the R-CD aqueous solutions, the absolute quantum yield and fluorescence lifetime of the quantum dots were measured, using a steady-state transient fluorescence spectrometer (FL3-111). In Figure S2C, the fluorescence decay of R-CDs occurring at 593 nm reveals a single exponential fitting curve with an average lifetime of 2.8 ns. The absolute quantum yield measured at an excitation wavelength of 500 nm is 2.67%. Likewise, the photoluminescence (PL) intensities are still above 90% after 60 min under continuous excitation at 500 nm, indicating that R-CDs exhibit excellent light stability (Figure S2D).

Subsequently, the elemental composition and the surface functional groups of R-CDs were further studied by X-ray photoelectron spectroscopy (XPS) and Fourier transform infrared (FT-IR). The full XPS spectra presented in Figure S3 show four typical peaks: S 2p (168 eV), C 1s (285 eV), N 1s (401 eV), and O 1s (532 eV), and their percentages are 4.5, 52.7, 27.7, and 15.1%, respectively. Figure 2 shows the high-resolution spectra of four elements. The C 1s band can be deconvoluted into three peaks, corresponding to sp^2 carbons (C═C, 284.7 eV), sp^3 carbons (C−N, 285.4 eV), and sp^3 carbons (C−S/C−O, 285.8 eV) (Figure 2A).[28,29] The N 1s band can be deconvoluted into three peaks at 399.2, 400, and 401.3 eV, representing pyridinic N, pyrrolic N, and amino N, respectively (Figure 2B).[30] The O 1s band contains two peaks at 531.1 and 532.2 eV for S−O and C−O, respectively (Figure 2C).[31] The S 2p XPS spectrum demonstrates three peaks centered at 168, 168.2, and 169.2 eV for the $-C-SO_x$ (x = 2, 3, and 4) species (Figure 2D).[32,33] The FT-IR spectrum of CDs displays a weak peak between 3125 and 3100 cm^{-1} and two characteristic peaks between 1600 and 1500 cm^{-1}, indicating the presence of a pyrrole structure. Three bands at the wavenumbers 1128, 1307, and 1413 cm^{-1} are characteristic absorption peaks of C−C stretching frequencies and C−H bending frequencies (Figure S4). The above results show that the N,S-co-doped R-CDs were synthesized and the surface of R-CDs were plentiful in amino, hydroxyl, and sulfhydryl groups, a necessary condition for R-CDs to have excellent optical properties and good water solubility.

2.2. Strategy of the Switch-On Detection of Fe^{3+} Ions and L-Cys. Based on the above characterization results of R-CDs, we found that the successful doping of N and S resulted in the presence of abundant functional groups on the surface of R-CDs. It prompted us to further investigate the potential sensing applications of R-CDs. It was found that Fe^{3+} ions have high quenching efficiency for the fluorescence of R-CDs. Further screening revealed that the presence of L-Cys could competitively bind Fe^{3+} ions, thus resulting in the PL recovery of R-CDs. More importantly, the entire sensing process can be

DOI: 10.1021/acsomega.9b01019
ACS Omega 2019, 4, 12575−12583

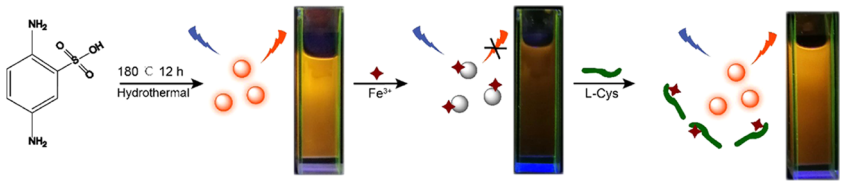

Figure 3. Schematic illustration of the switch-on dual function sensing platform for detecting Fe^{3+} ions and L-Cys.

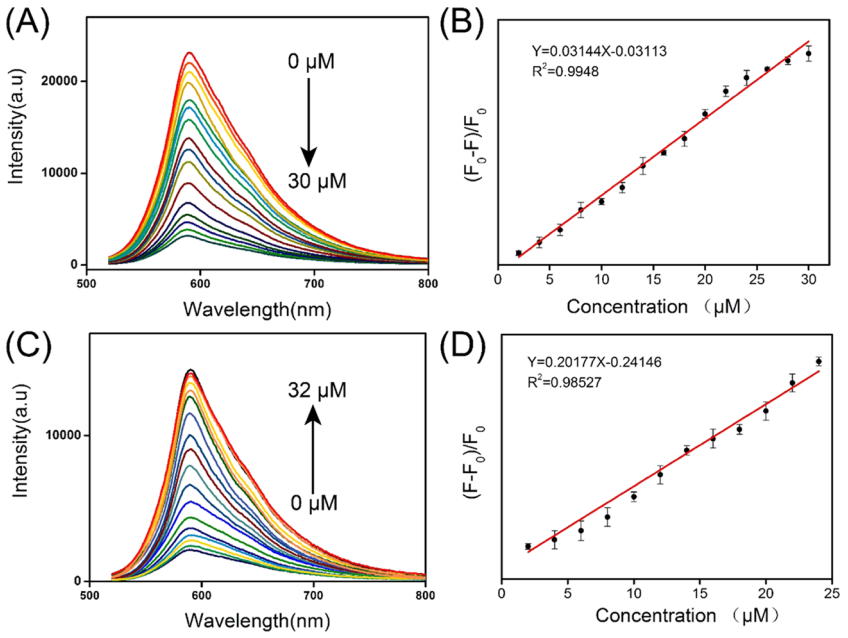

Figure 4. FL emission spectra of the R-CDs upon the addition of various concentrations of Fe^{3+} ions from 0 to 30 μM (A). Relationship between $(F_0 - F)/F_0$ and the concentration of Fe^{3+} ions, where F_0 and F are the FL intensities of the R-CDs in the absence and presence of Fe^{3+} ions, respectively (B). FL emission spectra of the aqueous R-CDs and Fe^{3+} (30 μM) mixture upon the addition of various concentrations of L-Cys from 0 to 32 μM (C). Relationship between $(F - F_0)/F_0$ and the concentration of L-Cys, where F_0 and F are the FL intensities of the aqueous R-CDs and Fe^{3+} mixture in the absence and presence of L-Cys, respectively (D).

completed in a few minutes. Therefore, we propose a switch-on dual function sensing platform for stepwise detection of Fe^{3+} ions and L-Cys. The schematic diagram of the entire inspection process is shown in Figure 3. The main reason why R-CDs can specifically recognize and quantify Fe^{3+} ions is that the surface of R-CDs is rich in N and S functional groups, which can effectively complex Fe^{3+} ions. Due to the formation of R-CDs/Fe^{3+} complexes, the electrons that promote the excited state of the R-CDs are transferred to the semifilled orbit of the Fe^{3+} ions, and therefore, the process of returning the excited state to the ground state is blocked, so that the fluorescence is quenched.[2,34−36] Furthermore, as shown in Figure S5, the absorption peak of R-CDs at 510 nm was shifted due to the addition of Fe^{3+} ions, also indicating that R-CDs form a complex with Fe^{3+} ions. However, after adding L-Cys to the R-CDs/Fe^{3+} system, it was found that the blue-shifted absorption peak recovered. This is attributed to the stronger complexation properties of L-Cys on Fe^{3+} ions than R-CDs.

2.3. Fe^{3+} Ions and L-Cys Detection Performance. L-Cys is one of the most important biothiols, and Fe^{3+} is also a crucial trace element. They play a significant role in human physiological processes. More importantly, L-Cys has a strong affinity for Fe^{3+} ions, which laid the foundation for us to design a switch-on fluorescent sensing platform for the quantitative detection of L-Cys. Therefore, we investigated the feasibility of detecting Fe^{3+} ions by measuring the FL intensity at 593 nm of an R-CD solution with various concentrations of Fe^{3+} ions. As shown in Figure 4A, increasing the concentration of Fe^{3+} ions caused a decrease in the fluorescence intensity of the R-CD system and the quenching efficiency $[(F_0 - F)/F_0]$ displayed a good linear relationship (R^2 = 0.9948) with the concentration of Fe^{3+} ions. The concentration range of Fe^{3+} ions is 0−30 μM, where F_0 and F are the FL intensities of the R-CDs in the absence and presence of Fe^{3+} ions, respectively. The fitted linear regression equation is $Y = 0.03144x - 0.03113$ (Figure 4B). The limit of detection (LOD) for Fe^{3+} is calculated to be 0.27 μM, based on 3 times the signal-to-noise criteria. By increasing the concentration of Fe^{3+} ions, the fluorescence is gradually annihilated by the naked eye under the illumination of a 450 nm light-emitting diode (LED) lamp (Figure S6). Subsequently, Fe^{3+} ions with a concentration of 30 μM were selected as the best quenching dose according to the quenching degree and quenching efficiency of R-CD fluorescence. When different concentrations of L-Cys were introduced into the R-CDs/Fe^{3+} system, the fluorescence of the R-CDs/Fe^{3+}/L-Cys system gradually recovered as the concentration of L-Cys increased, as shown in Figure 4C. Furthermore, the recovery efficiency $[(F_0 - F)/F_0]$ revealed a good linear relationship (R^2 = 0.98527) with the concentration of L-Cys. The concentration range of L-Cys is 0−24 μM, where F_0 and F are the fluorescence intensities of the aqueous R-CDs and Fe^{3+} mixture in the absence and presence of L-Cys,

DOI: 10.1021/acsomega.9b01019
ACS Omega 2019, 4, 12575−12583

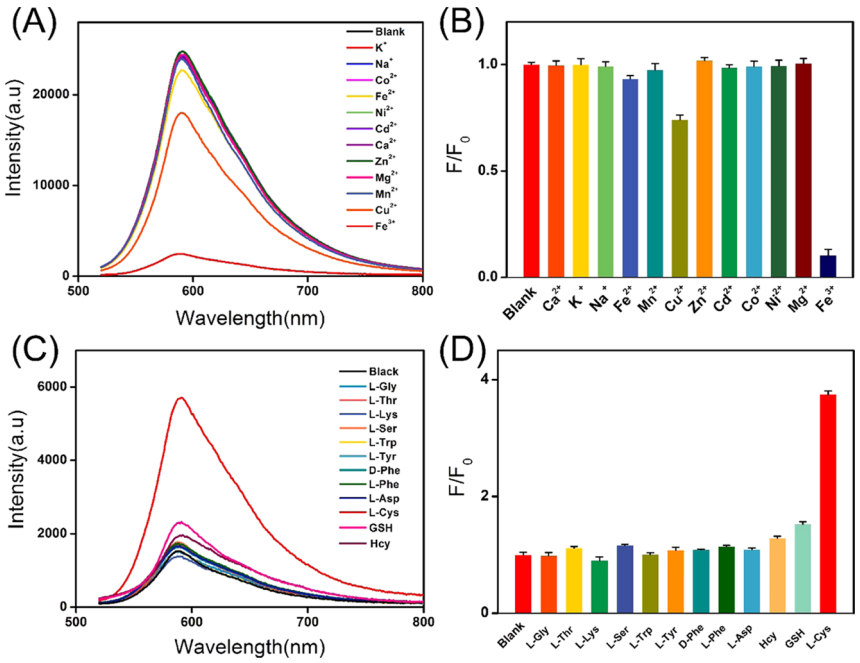

Figure 5. FL emission intensity (A) and F/F_0 (B) of aqueous R-CD solution in the presence of various metal ions, where F_0 and F are the FL intensities of the R-CDs in the absence and presence of various metal ions. FL emission intensity (C) and F/F_0 (D) of the aqueous R-CDs and Fe^{3+} mixture in the presence of various amino acids, where F_0 and F are the FL intensities of the aqueous R-CDs and Fe^{3+} mixture in the absence and presence of various amino acids.

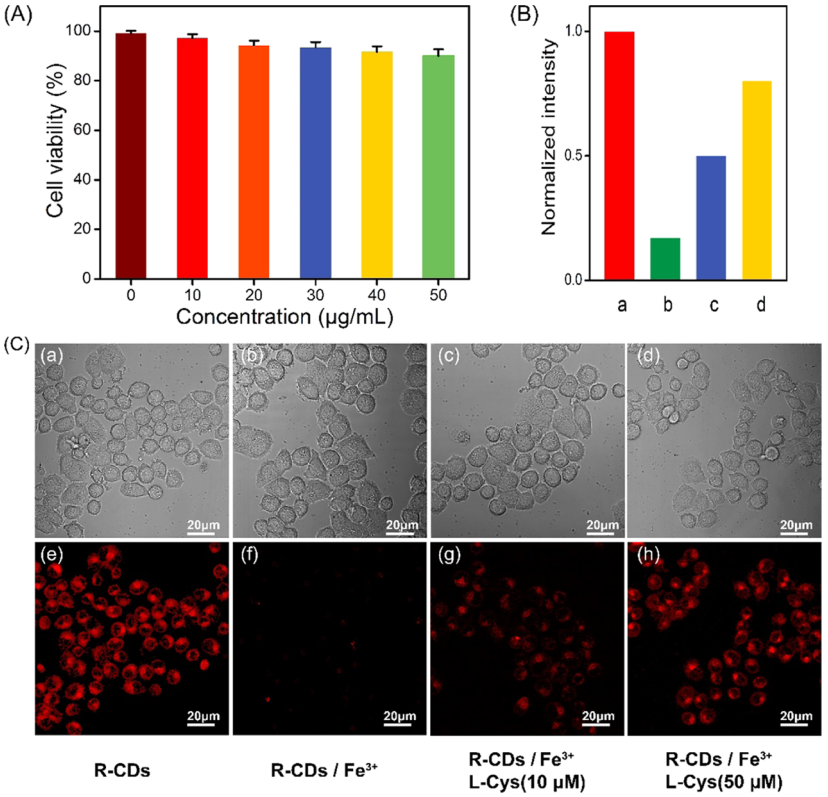

Figure 6. (A) Cellular cytotoxicity assessment of the R-CDs using the standard MTT assay toward Hep G2 cells. (B) Normalized fluorescence intensity of (e)−(h) of (C). (C) Confocal fluorescence images (e−h) and bright-field images (a−d) of HeP G2 cells incubated with R-CDs (a), R-CDs/Fe^{3+} (b), R-CDs/Fe^{3+}/L-Cys (10 μM) (c), and R-CDs/Fe^{3+}/L-Cys (50 μM) (d).

respectively (Figure 4D). Furthermore, the LOD for L-Cys is calculated to be 0.14 μM according to 3 times the signal-to-noise criteria. When different concentrations of L-Cys were introduced into the R-CDs/Fe^{3+} system, it was observed with the naked eye that the fluorescence gradually recovered with the increase of the concentration of L-Cys under the illumination of a 450 nm LED lamp (Figure S7). Finally, the optimal reaction time of the fluorescence quenching of R-CDs

DOI: 10.1021/acsomega.9b01019
ACS Omega 2019, 4, 12575−12583

by Fe^{3+} ions and the fluorescence recovery of L-Cys to the R-CDs/Fe^{3+} system were investigated (Figures S8 and S9). It has been found that both reactions can be completed in less than 1 min, which means that the detection system can monitor Fe^{3+} ions and L-Cys in real time.

2.4. Selectivity of R-CDs for Fe^{3+} Ions and L-Cys Detection. To assess the selectivity of the sensor platform for Fe^{3+} ions and L-Cys, first, the fluorescence spectra of the aqueous solution of R-CDs that coexisted with different metal ions (Ag^{+}, Cu^{2+}, Pb^{2+}, Fe^{3+}, Fe^{2+}, Zn^{2+}, Cd^{2+}, Ni^{2+}, Co^{2+}, Mg^{2+}, Al^{3+}, Ca^{2+}, Na^{+}, K^{+}, and Mn^{2+}) were recorded under the excitation of 500 nm. It is interesting to note in Figure 5A,B that the luminescence intensity of the R-CDs is nearly 90%, quenched by Fe^{3+} ions. However, approximately 30% of the fluorescence intensity can be quenched by the same concentration of Cu^{2+} ions. In addition, when other metal ions are added to the aqueous solution of R-CDs, there is no significant difference in fluorescence intensity, which indicates that the R-CDs have good selectivity to Fe^{3+} ions and can be used for the specific identification of Fe^{3+} ions. Furthermore, various amino acid (L-Gly, L-Thr, L-Lys, L-Ser, L-Trp, L-Tyr, D-Phe, L-Phe, L-Asp, Hcy, and GSH) interferences were investigated. As shown in Figure 5C,D, these interferents caused little recovery of fluorescence, while the same concentration of L-Cys could recover about 4 times the initial fluorescence intensity, indicating that the sensing platform has excellent sensitivity and specificity. It is important to point out that the entire process can be completed in a few minutes, and therefore, the sensing platform is sensitive and efficient.

2.5. Real Sample Detection. To evaluate the potential practical value of R-CDs as recognition elements, different concentrations of Fe^{3+} ions and L-Cys were added to pretreated human serum samples to verify the method, respectively. As shown in Table S1, the standard deviation of human serum samples with different concentrations of Fe^{3+} ions was less than 2.32, and the recovery range was 98.60−103.8%. Table S2 shows that the relative standard deviation of human serum samples spiked with L-Cys was less than 2.16 and the recovery was between 98.3 and 101%. The above results indicate that the sensing platform shows excellent performance in actual sample detection.

2.6. Cytotoxicity of R-CDs and Fe^{3+} and L-Cys Sensing in Living Cells. Due to its excellent FL behavior and fascinating stability, R-CD is an ideal candidate for bioimaging. To test the characteristic cell cytotoxicity of the R-CDs, we first carried out the standard 3-(4,5-dimethyldiazol-2-yl)-2,5-diphenyltetrazolium bromide (MTT) assays. The results (Figure 6A) showed that more than 90% of the cells survived after 24 h of incubation with R-CDs at a concentration of 10−50 $\mu g\ mL^{-1}$, which indicates that R-CDs have no obvious cytotoxicity. So, we assessed the in vitro imaging performance of R-CDs on Hep G2 cells. As shown in Figure S10, after incubation with R-CDs (20 $\mu g\ mL^{-1}$) for 2 h, the shape of these cells were retained and the Hep G2 cells could emit intense red fluorescence under 405 nm laser excitation. The above results indicate that R-CDs are endocytosed into the cytoplasm due to excellent biocompatibility. What is more interesting is that our previous switch-on design for detecting Fe^{3+} ions and L-Cys can also be implemented in the Hep G2 cells. First, Hep G2 cells were incubated with R-CDs for 2 h. After washing off the excess R-CDs, the confocal microscopy images were captured immediately (Figure 6C(a,e)). Then, the concentration of 30 μM Fe^{3+} ion solution was added into the R-CD pretreated cells. After washing the cells three times with phosphate-buffered saline (PBS) buffer solution, confocal microscopy images were captured after fixing with 500 μL of PBS buffer. It is observed that the red fluorescence was obviously quenched (Figure 6C(b,f)). Subsequently, we introduced 10 μM (Figure 6C(c,g)) and 50 μM (Figure 6C(d,h)) of L-Cys in the same way and found that the fluorescence of R-CDs in the cells gradually recovered. Figure 6B shows the normalized fluorescence intensity captured at various stages of the process, indicating that the detection system provides the possibility of visual monitoring of intracellular Fe^{3+} ions and L-Cys, in view of the fact that R-CDs can emit excitation-independent bright red fluorescence.

2.7. In Vivo Imaging. To confirm that R-CDs have good tissue penetration, in vivo nude mouse imagings were captured. As shown in Figure S11, 100 μL of R-CD aqueous solution was injected subcutaneously and the fluorescence intensity at different emission wavelengths was captured under excitation at 535 nm. It was found that bright fluorescence at the injection site was observed at 600 nm (Figure 7). The mice injected with physiological saline were used as controls. Therefore, dual-functional sensing platforms based on good tissue-penetrating R-CDs have potential applications in in vivo monitoring.

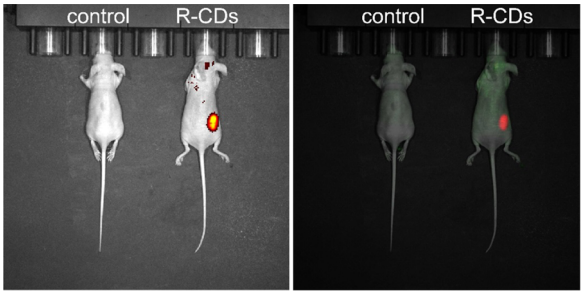

Figure 7. In vivo PL images of nude mice were injected subcutaneously with 100 μL of saline and 100 μL of an aqueous solution of R-CDs, respectively.

3. CONCLUSIONS

In summary, moderate quantum yields of red luminescent carbon dots codoped with sulfur and nitrogen were prepared by a facile hydrothermal method using 2,5-diaminobenzenesulfonic acid as the unique carbon source. R-CDs showed excitation-independent bright red fluorescence and were successfully applied to cell imaging as well as in vivo imaging in mice, indicating that the as-prepared R-CDs have excellent tissue penetration and cell labeling ability. More interestingly, R-CDs can be used to construct a dual-functional sensing platform for high-sensitivity real-time detection of Fe^{3+} ions and L-Cys due to the doping of nitrogen and sulfur to impart a rich functional group on the surface of the R-CDs. The linear detection range of Fe^{3+} is 0−30 μM (LOD: 0.27 μM), and the detection range of L-Cys is 0−24 μM (LOD: 0.14 μM). The sensor platform was used to detect Fe^{3+} ions and L-Cys in human serum samples with satisfactory results. It is worth mentioning that the switch-on fluorescence behavior for cell imaging by reacting with Fe^{3+} ions and L-Cys, respectively, has been investigated, which provides the possibility of real-time monitoring in vivo.

DOI: 10.1021/acsomega.9b01019
ACS Omega 2019, 4, 12575−12583

4. EXPERIMENTAL SECTION

4.1. Materials. Reagent grades of 2,5-diaminobenzenesulfonic acid was acquired from Sigma-Aldrich (St. Louis, MO). Fetal bovine serum, analytical grade 3-(4,5-dimethyldiazol-2-yl)-2,5-diphenyltetrazolium bromide (MTT), and Dulbecco's modified Eagle medium (DMEM) were also purchased from Sigma-Aldrich (St. Louis, MO). All solutions were prepared with deionized (DI) water from a Milli-Q-RO4 water purification system (Millipore).

4.2. Instrumentation and Characterization. Excitation and emission spectra were recorded using a fluorescence spectrophotometer (F-7000, Hitachi). Fluorescence imaging physical photos were excited by an LED lamp at 450 nm (LUYOR-3260RB, Shanghai LUYOR Instrument Co., Ltd). UV−vis absorption spectra were recorded on an Avaspec-2048 UV−vis spectrophotometer. Powder X-ray diffraction spectra (PXRD) was obtained on a PANalytical B.V. (Netherlands) X'PERT PXRD. Fourier transform infrared spectra (FT-IR) were measured on a Thermo FT-IR spectrophotometer. The images of high-resolution transmission electron microscopy (HRTEM) were captured on a JEM-2100 (JEOL, Japan) electron microscope operating at 200 kV. X-ray photoelectron spectra (XPS) were obtained on KRATOS XSAM800 X-ray photoelectron spectrometer (Kratos Analytical Ltd, Manchester), using Mg as the excitation source. Raman spectra were collected on an Alpha300 WiTec Raman microscope (Witec Inc., Ulm, Germany). PL lifetime and QYs were measured using FL3-111 (HORIBA Instruments). The MTT assay was measured with a microplate reader (Spectra MAX 340, Molecular Devices Co., Sunnyvale, CA). Confocal optical micrographs were captured using a confocal laser scanning microscope (CarlZeiss LSM710, Oberkochen, Germany). Fluorescence images were recorded using an IVIS Spectrum CT small animal imaging system (Caliper Life Sciences, Hopkinton, MA).

4.3. Synthesis of R-CDs. Precisely, 0.09 g of 2,5-diaminobenzenesulfonic acid was dissolved in 30 mL of DI water and the solution was transferred into a 50 mL Teflon autoclave. The autoclave was heated at 200 °C for 10 h and then naturally cooled down to room temperature. Subsequently, the red-brown suspension was centrifuged at 14 000 rpm for 10 min to precipitate large particles and the supernatant was dialyzed against a dialysis bag (500 Da) for 24 h to remove the raw material. A reddish-brown powder was obtained by freeze drying and was stored at 4 °C.

4.4. Quantum Yield (QY) Measurements. Measurement was taken of the absolute QYs using a steady-state transient fluorescence spectrometer (FL3-111). First, the optimum concentration was adjusted according to the absorption intensity of the R-CD aqueous solution at an excitation wavelength of 500 nm. Second, the solution was introduced into a 1 cm fluorescence cuvette for QY measurement. Meanwhile, the same fluorescence spectra of pure water were also obtained under the same conditions. Finally, the QYs were calculated using fluorescence software.

4.5. Detection of Fe^{3+} Ions and L-Cys. To achieve quantitative detection of Fe^{3+} ions, 100 μL of different concentrations of Fe^{3+} solution were added to 900 μL of R-CD solution. The fluorescence intensity was measured with the same procedure as before to examine the detection range of R-CDs for Fe^{3+} ions. The solutions containing different metal ions (Ag^{+}, Cu^{2+}, Pb^{2+}, Fe^{3+}, Fe^{2+}, Zn^{2+}, Cd^{2+}, Ni^{2+}, Co^{2+}, Mg^{2+}, Al^{3+}, Ca^{2+}, Na^{+}, K^{+}, and Mn^{2+}) were prepared and then thoroughly mixed with the R-CD solution. After standing for 30 s, the fluorescence intensity of the mixed solution was measured by a fluorescence spectrophotometer to examine the selectivity of the R-CDs to the metal ions. To detect L-Cys, 100 μL of different concentrations of L-Cys solution were added to 900 μL of R-CDs/Fe^{3+} mixture and the fluorescence intensity of the mixed system was recorded. To evaluate the selectivity of the sensor for L-Cys, they were replaced with different interfering agents under the same experimental conditions. All samples were tested at an excitation wavelength of 500 nm and an emission wavelength of 593 nm.

4.6. MTT Assays. The 3-(4,5-dimethylthiazol-2-yl)-2,5-diphenyltetrazolium bromide (MTT) assay was employed for the evaluation of cytotoxicity of synthesized R-CDs. Hep G2 cells (5×10^4 cells per well) were seeded in 96-well cultured plates and incubated for 24 h with 5% CO_2 at 37 °C. The cells were then exposed to different concentrations (0−50 μg mL^{-1}) of R-CDs and further incubated for 24 h in the absence of DMEM. The cells were washed with PBS solution and treated with 20 μL of MTT solution for 4 h. Then, the insoluble precipitate of MTT (formazan) was dissolved in dimethyl sulfoxide. Finally, the optical absorbance was detected at 570 nm.

4.7. In Vitro/Vivo Imaging. Cellular fluorescence images were captured using an LSM710 laser scanning confocal microscope at ambient temperature. In brief, 500 μL of Hep G2 cells (5×10^5 cells per mL) in DMEM with 10% fetal bovine serum were seeded into 4-well culture plates and incubated at 37 °C in a 5% CO_2 incubator for 24 h. Subsequently, the culture source was substituted with a mixture of the R-CDs (20 μg mL^{-1}) in DMEM, followed by the incubation of Hep G2 cells for 2 h. After removing the supernatant, Hep G2 cells were washed three times with PBS buffer solution to remove the free R-CDs and then fixed with 500 μL of PBS buffer.[37]

Fluorescence images of mice were captured at 600 nm using an IVIS Spectrum CT small animal imaging system under an excitation wavelength of 535 nm. In vivo imaging performance of R-CDs was observed by subcutaneous injection of 100 μL (50 μg mL^{-1}) of an aqueous solution of R-CDs in nude mice.

■ ASSOCIATED CONTENT

Supporting Information

The Supporting Information is available free of charge on the ACS Publications website at DOI: 10.1021/acsomega.9b01019.

FL emission spectra of the R-CDs obtained under different reaction conditions (Figure S1); characterization of the R-CDs (Figures S2−S4); UV−vis spectra of R-CDs in the presence of Fe^{3+} and addition of L-Cys (Figure S5); photographs of the detection system in the presence of different concentrations of Fe^{3+} ions and L-Cys under 450 nm LED lamp irradiation (Figures S6 and S7); time course of quenching and restoration of the fluorescence of R-CDs (Figures S8 and S9); confocal fluorescence images of Hep G2 cells incubated with R-CDs (Figure S10); in vivo PL images of nude mice at different emission wavelengths (Figure S11); and sample detection results (Tables S1 and S2) (PDF)

DOI: 10.1021/acsomega.9b01019
ACS Omega 2019, 4, 12575−12583

AUTHOR INFORMATION

Corresponding Authors

*E-mail: sunjiadi@jiangnan.edu.cn (J.S.).
*E-mail: sxlzyz@jiangnan.edu.cn (X.S.).

ORCID

Xiulan Sun: 0000-0003-1528-8601

Notes

The authors declare no competing financial interest.

ACKNOWLEDGMENTS

This work has been supported by the National Research Program of China (Nos. 2016YFD0401204, 31772069, YZ201709), Agricultural Science and Technology indigenous Innovation Program of Jiangsu Province (No. CX (17)10032), National First-class Discipline Program of Food Science and Technology (No. JUFSTR20180303), and Fundamental Research Funds for the Central Universities (No. JUSRP11906).

REFERENCES

(1) Li, P.; Zhang, M.; Sun, X.; Guan, S.; Zhang, G.; Baumgarten, M.; Müllen, K. A dendrimer-based highly sensitive and selective fluorescence-quenching sensor for Fe^{3+} both in solution and as film. *Biosens. Bioelectron.* **2016**, *85*, 785−791.

(2) Huang, Q.; Li, Q.; Chen, Y.; Tong, L.; Lin, X.; Zhu, J.; Tong, Q. High quantum yield nitrogen-doped carbon dots: green synthesis and application as "off-on" fluorescent sensors for the determination of Fe^{3+} and adenosine triphosphate in biological samples. *Sens. Actuators, B* **2018**, *276*, 82−88.

(3) Edison, T. N. J. I.; Atchudan, R.; Shim, J.-J.; Kalimuthu, S.; Ahn, B.-C.; Lee, Y. R. Turn-off fluorescence sensor for the detection of ferric ion in water using green synthesized N-doped carbon dots and its bio-imaging. *J. Photochem. Photobiol., B* **2016**, *158*, 235−242.

(4) Zong, J.; Yang, X.; Trinchi, A.; Hardin, S.; Cole, I.; Zhu, Y.; Li, C.; Muster, T.; Wei, G. Carbon dots as fluorescent probes for "off-on" detection of Cu^{2+} and L-cysteine in aqueous solution. *Biosens. Bioelectron.* **2014**, *51*, 330−335.

(5) Wei, X.; Hu, H.; Zheng, B.; Arslan, Z.; Huang, H.-C.; Mao, W.; Liu, Y.-M. Profiling metals in Cordyceps sinensis by using inductively coupled plasma mass spectrometry. *Anal. Methods* **2017**, *9*, 724−728.

(6) Grindlay, G.; Gras, L.; Hernandis, V.; Mora, J. On-line microwave-based preconcentration device for inductively coupled plasma atomic emission spectrometry: Application to the elemental analysis of spirit samples. *Talanta* **2013**, *107*, 11−17.

(7) Sinner, T.; Hoffmann, P.; Ortner, H. Determination of Fe (II) and Fe (III) in small samples by microbore ion chromatography and photometric, atomic absorption spectrometry and total-reflection X-ray fluorescence detection. *Spectrochim. Acta, Part B* **1993**, *48*, 255−261.

(8) Stachniuk, J.; Kubalczyk, P.; Furmaniak, P.; Głowacki, R. A versatile method for analysis of saliva, plasma and urine for total thiols using HPLC with UV detection. *Talanta* **2016**, *155*, 70−77.

(9) Ivanov, A. V.; Bulgakova, P. O.; Virus, E. D.; Kruglova, M. P.; Alexandrin, V. V.; Gadieva, V. A.; Luzyanin, B. P.; Kushlinskii, N. E.; Fedoseev, A. N.; Kubatiev, A. A. Capillary electrophoresis coupled with chloroform-acetonitrile extraction for rapid and highly selective determination of cysteine and homocysteine levels in human blood plasma and urine. *Electrophoresis* **2017**, *38*, 2646−2653.

(10) Song, Y.; Zhu, C.; Song, J.; Li, H.; Du, D.; Lin, Y. Drug-derived bright and color-tunable N-doped carbon dots for cell imaging and sensitive detection of Fe^{3+} in living cells. *ACS Appl. Mater. Interfaces* **2017**, *9*, 7399−7405.

(11) Li, H.; Yan, X.; Qiao, S.; Lu, G.; Su, X. Yellow-emissive carbon dot-based optical sensing platforms: cell imaging and analytical applications for biocatalytic reactions. *ACS Appl. Mater. Interfaces* **2018**, *10*, 7737−7744.

(12) Huang, P.; Lin, J.; Wang, X.; Wang, Z.; Zhang, C.; He, M.; Wang, K.; Chen, F.; Li, Z.; Shen, G.; et al. Light-triggered theranostics based on photosensitizer-conjugated carbon dots for simultaneous enhanced-fluorescence imaging and photodynamic therapy. *Adv. Mater.* **2012**, *24*, 5104−5110.

(13) Lim, S. Y.; Shen, W.; Gao, Z. Carbon quantum dots and their applications. *Chem. Soc. Rev.* **2015**, *44*, 362−381.

(14) Wang, J.; Qiu, J. A review of carbon dots in biological applications. *J. Mater. Sci.* **2016**, *51*, 4728−4738.

(15) Bao, R.; Chen, Z.; Zhao, Z.; Sun, X.; Zhang, J.; Hou, L.; Yuan, C. Green and facile synthesis of nitrogen and phosphorus co-doped carbon quantum dots towards fluorescent ink and sensing applications. *Nanomaterials* **2018**, *8*, 386.

(16) Liu, H.; Sun, Y.; Yang, J.; Hu, Y.; Yang, R.; Li, Z.; Qu, L.; Lin, Y. High performance fluorescence biosensing of cysteine in human serum with superior specificity based on carbon dots and cobalt-derived recognition. *Sens. Actuators, B* **2019**, *280*, 62−68.

(17) Huang, H.; Weng, Y.; Zheng, L.; Yao, B.; Weng, W.; Lin, X. Nitrogen-doped carbon quantum dots as fluorescent probe for "off-on" detection of mercury ions, L-cysteine and iodide ions. *J. Colloid Interface Sci.* **2017**, *506*, 373−378.

(18) Chen, K.; Qing, W.; Hu, W.; Lu, M.; Wang, Y.; Liu, X. On-off-on fluorescent carbon dots from waste tea: Their properties, antioxidant and selective detection of CrO_4^{2-}, Fe^{3+}, ascorbic acid and L-cysteine in real samples. *Spectrochim. Acta, Part A* **2019**, *213*, 228−234.

(19) Zhang, Y.; Cui, P.; Zhang, F.; Feng, X.; Wang, Y.; Yang, Y.; Liu, X. Fluorescent probes for "off-on" highly sensitive detection of Hg^{2+} and L-cysteine based on nitrogen-doped carbon dots. *Talanta* **2016**, *152*, 288−300.

(20) Devi, S.; Kaur, A.; Sarkar, S.; Vohra, S.; Tyagi, S. Synthesis and characterization of highly luminescent N-doped carbon quantum dots for metal ion sensing. *Integr. Ferroelectr.* **2018**, *186*, 32−39.

(21) Yang, Y.; Huo, D.; Wu, H.; Wang, X.; Yang, J.; Bian, M.; Ma, Y.; Hou, C. N, P-doped carbon quantum dots as a fluorescent sensing platform for carbendazim detection based on fluorescence resonance energy transfer. *Sens. Actuators, B* **2018**, *274*, 296−303.

(22) Ding, H.; Yu, S.-B.; Wei, J.-S.; Xiong, H.-M. Full-color light-emitting carbon dots with a surface-state-controlled luminescence mechanism. *ACS Nano* **2016**, *10*, 484−491.

(23) Gude, V.; Das, A.; Chatterjee, T.; Mandal, P. K. Molecular origin of photoluminescence of carbon dots: aggregation-induced orange-red emission. *Phys. Chem. Chem. Phys.* **2016**, *18*, 28274−28280.

(24) Qu, Z.; Na, W.; Nie, Y.; Su, X. A novel fluorimetric sensing strategy for highly sensitive detection of phytic acid and hydrogen peroxide. *Anal. Chim. Acta* **2018**, *1039*, 74−81.

(25) Miao, X.; Yan, X.; Qu, D.; Li, D.; Tao, F. F.; Sun, Z. Red emissive sulfur, nitrogen codoped carbon dots and their application in ion detection and theraonostics. *ACS Appl. Mater. Interfaces* **2017**, *9*, 18549−18556.

(26) Liu, Y.; Duan, W.; Song, W.; Liu, J.; Ren, C.; Wu, J.; Liu, D.; Chen, H. Red emission B, N, S-co-doped carbon dots for colorimetric and fluorescent dual mode detection of Fe^{3+} ions in complex biological fluids and living cells. *ACS Appl. Mater. Interfaces* **2017**, *9*, 12663−12672.

(27) Zhang, F.; Liu, F.; Wang, C.; Xin, X.; Liu, J.; Guo, S.; Zhang, J. Effect of lateral size of graphene quantum dots on their properties and application. *ACS Appl. Mater. Interfaces* **2016**, *8*, 2104−2110.

(28) Murugan, N.; Prakash, M.; Jayakumar, M.; Sundaramurthy, A.; Sundramoorthy, A. K. Green synthesis of fluorescent carbon quantum dots from Eleusine coracana and their application as a fluorescence 'turn-off' sensor probe for selective detection of Cu^{2+}. *Appl. Surf. Sci.* **2019**, *476*, 468−480.

(29) Shen, P.; Xia, Y. Synthesis-modification integration: one-step fabrication of boronic acid functionalized carbon dots for fluorescent blood sugar sensing. *Anal. Chem.* **2014**, *86*, 5323−5329.

(30) Song, Z.; Quan, F.; Xu, Y.; Liu, M.; Cui, L.; Liu, J. Multifunctional N, S co-doped carbon quantum dots with pH- and

DOI: 10.1021/acsomega.9b01019
ACS Omega 2019, 4, 12575−12583

thermo-dependent switchable fluorescent properties and highly selective detection of glutathione. *Carbon* **2016**, *104*, 169−178.
(31) Khare, P.; Bhati, A.; Anand, S. R.; Gunture; Sonkar, S. K. Brightly fluorescent zinc-doped red-emitting carbon dots for the sunlight-induced photoreduction of Cr (VI) to Cr (III). *ACS Omega* **2018**, *3*, 5187−5194.
(32) Yang, G.; Wan, X.; Su, Y.; Zeng, X.; Tang, J. Acidophilic S-doped carbon quantum dots derived from cellulose fibers and their fluorescence sensing performance for metal ions in an extremely strong acid environment. *J. Mater. Chem. A* **2016**, *4*, 12841−12849.
(33) Yao, Y.; Guo, Y.; Du, W.; Tong, X.; Zhang, X. In situ synthesis of sulfur-doped graphene quantum dots decorated carbon nanoparticles hybrid as metal-free electrocatalyst for oxygen reduction reaction. *J. Mater. Sci.: Mater. Electron.* **2018**, *29*, 17695−17705.
(34) Han, C.; Wang, R.; Wang, K.; Xu, H.; Sui, M.; Li, J.; Xu, K. Highly fluorescent carbon dots as selective and sensitive "on-off-on" probes for iron (III) ion and apoferritin detection and imaging in living cells. *Biosens. Bioelectron.* **2016**, *83*, 229−236.
(35) Zhu, S.; Meng, Q.; Wang, L.; Zhang, J.; Song, Y.; Jin, H.; Zhang, K.; Sun, H.; Wang, H.; Yang, B. Highly photoluminescent carbon dots for multicolor patterning, sensors, and bioimaging. *Angew. Chem., Int. Ed.* **2013**, *52*, 3953−3957.
(36) Gong, X.; Lu, W.; Paau, M. C.; Hu, Q.; Wu, X.; Shuang, S.; Dong, C.; Choi, M. M. Facile synthesis of nitrogen-doped carbon dots for Fe^{3+} sensing and cellular imaging. *Anal. Chim. Acta* **2015**, *861*, 74−84.
(37) Gao, T.; Wang, X.; Yang, L.-Y.; He, H.; Ba, X.-X.; Zhao, J.; Jiang, F.-L.; Liu, Y. Red, yellow, and blue luminescence by graphene quantum dots: syntheses, mechanism, and cellular imaging. *ACS Appl. Mater. Interfaces* **2017**, *9*, 24846−24856.

DOI: 10.1021/acsomega.9b01019
ACS Omega 2019, 4, 12575−12583